# Influence of carbonate impurities on smartwater effect: evaluation of wettability alteration process by geochemical simulation

Xingjuan Hao [1], Moataz Abu-Al-Saud [2], Subhash Ayirala [2], Yogarajah Elakneswaran [1, *]

[1] Division of Sustainable Resources Engineering

Faculty of Engineering, Hokkaido University

Kita 13, Nishi 8, Kita-ku, Sapporo, 060-8628, Japan

[2] EXPEC Advanced Research Center, Saudi Aramco, Dhahran 31311, Saudi Arabia

* Corresponding author

E-mail: elakneswaran@eng.hokudai.ac.jp

Tel: +81-11-706-7274

**Highlights**

- Equilibrium of carbonate impurities contributed to carbonate/brine than oil/brine.
- Brine with $SO_4^{2-}$ results in higher water-wet condition compared to other solutions.
- The measured adhesion force is inversely related to calculated disjoining pressure.
- An increase of -COOH/-NH ratio shows more water-wet state.

**Abstract**

Low salinity water flooding (LSWF) has been considered as a promising technique for enhanced oil recovery (EOR). The wettability alteration towards a more water-wet state is recognised as the main mechanism for the positive LSWF effect. Electrokinetic interactions occurring at crude oil/brine and rock/brine interfaces affect the wettability alteration. Most of the studies reported in the existing knowledge considered synthetic calcite to understand the electrokinetics of natural carbonate with brines. The mineral impurities present in natural carbonate could influence the electrokinetics and subsequently wettability alteration. In this study, the surface complexation model, thermodynamic equilibrium model, and extended Derjaguin-Landau-Verwey-Overbeek (DLVO) theory were combined to evaluate the effect of impurities (dolomite and anhydrite) in natural carbonate on wettability alteration. The surface complexation modelling parameters were first estimated by fitting the calculated zeta potential to that of measured value in various brines and then validated in smartwater. The thermodynamic equilibrium of impurities is largely insensitive to crude oil/brine interface properties. However, the calculated carbonate/brine surface or zeta potential changed from positive to negative with anhydrite equilibrium in the brines containing $Ca^{2+}$ or $Mg^{2+}$ ions. The attractive or repulsive forces between crude oil and carbonate were estimated from disjoining pressure using extended DLVO theory and compared with measured adhesion forces. The computed disjoining pressure was used as an indicator to evaluate wettability alteration. It is found that brine with $SO_4^{2-}$ ions can result in highest water-wet condition, followed by smartwater (brine with $Ca^{2+}$, $Mg^{2+}$, and $SO_4^{2-}$) and brine with either $Ca^{2+}$ ions or $Mg^{2+}$ ions. The de-ionic (DI) water is unfavourable for wettability alteration. The effect of impurities equilibrium and the crude oil surface site densities on the disjoining pressure were also discussed.

**Keywords:** Triple-layer surface complexation model; Zeta potential; Smartwater; Carbonate impurities; Disjoining pressure; Adhesion force

## 1. Introduction

More than 60% of crude oil is present in carbonate reservoirs, most of which were described as naturally fractured and oil-wet [1,2]. Due to low recovery efficiency with conventional waterflooding, many enhanced oil recovery technologies have been investigated for tertiary oil recovery [3-11]. Low salinity water flooding (LSWF) or smartwater flooding (SWF) has recently attracted more attention for enhanced oil recovery (EOR) due to its low cost and eco-friendly nature. Various mechanisms such as fines migration, permeability reduction, osmotic effects, viscoelasticity, micro-dispersion formation, mineral dissolution, pH, desorption of polar oil components, expansion of electrical double layer (EDL), multi-component ionic exchange (MIE), and wettability alteration have been proposed for the positive effect of smartwater flooding [12-24]. However, the dominant mechanism is still uncertain, which can hinder the mechanistic modelling to accurately guide the design and implementation of this recovery technology for large-scale applications in different reservoirs.

Some researchers have recognized wettability alteration as a major physiochemical process for LSWF effect, which was affected by different factors including ionic composition and interface properties. Divalent potential determining ions (PDIs) of calcium, magnesium, sulphate have a significant influence on wettability alteration. Karimi et al. investigated the impact of $Mg^{2+}$, $SO_4^{2-}$, and cationic surfactant on wettability alteration in calcite [25]. Their results showed that both $Mg^{2+}$ and $SO_4^{2-}$ could act as wettability modifying agents for the oil-wet calcite, and the modified low salinity brine solutions effectively changed the wettability towards more water-wet state. Purswani and Karpyn conducted a series of waterflooding experiments using synthetic high salinity water and observed that the surface charge of limestone rocks was linearly affected by $Ca^{2+}$, $Mg^{2+}$, and $SO_4^{2+}$ ions [26]. In general, crude oil is negatively charged due to the dissociation of carboxylate groups (–COOH) whereas calcite, the main composition of carbonate, is positively charged [9,11]. These opposing surface charges result in the strong affinity of crude oil to the calcite surface to develop the oil-wet conditions.

Reservoir carbonate rocks are primarily composed of calcite ($CaCO_3$), dolomite ($CaMg(CO_3)_2$), and other impurities including quartz, anhydrite, clay minerals, organic matter, and apatite [27]. To further understand the electrostatic properties of carbonate reservoirs, limestone was widely studied. Song et al. selected Indiana limestone as the representative of carbonate minerals to evaluate the effect of ions on "smart water"-induced carbonate wettability alteration [28]. That study used zeta potential experiments, disjoining pressure, and surface complexation modelling to evaluate the electrostatic interactions. In addition, Alroudhan et al. studied the electrostatic properties of Portland limestone [29]. Their measured zeta potential was negative at high pCa or pMg (i.e., low $Ca^{2+}$ or $Mg^{2+}$ concentration) and become less negative with decreasing pCa or pMg. Tetteh et al. analysed the effect of several factors including ionic composition, temperature, and solution pH on Indiana limestone rock system and used double layer surface complexation model (SCM) of calcite/brine interface to predict zeta potentials of limestone [30]. In addition, they evaluated the significance of magnesium ions in the solution for EOR in limestone rock through wettability alteration [31]. The magnesium ions had a positive effect on wettability alteration whereas calcium ions had a detrimental effect. In these studies [30, 31], they did not analyse the effect of limestone impurities on the results, which might affect the magnesium concentration in the solution. Mahani et al. conducted a detailed experimental and surface complexation modelling study to examine the effect of rock type, brine composition and pH on the electrokinetics of carbonate/brine interface [32]. In this study [32], the surface complexation model and the parameters were considered for calcite surface to understand the measured zeta potential. Brady and Thyne used a double layer SCM based on calcite surface to predict oil recovery trends in carbonate reservoir [33]. Chen et al. study showed that surface chemistry of oil/brine and calcite/brine strongly affects the wettability of oil-brine-carbonate system [34], which is governed by crude oil composition and water chemistry. However, they did not evaluate the effect of carbonate impurities (quartz and ankerite) on the resulting of water chemistry changes.

The zeta potential of the natural carbonate is typically more negative than that of synthetic calcite or pure calcite crystal such as Iceland spar [35], which indicates the impurities significantly affected the surface chemistry of natural carbonate. However, only a few studies have been reported to evaluate the effect of impurities on the surface charge of natural carbonate. The influence of organic carboxylic acids and inorganic silica impurities was evaluated by using an extended SCM [35]. The presence of anhydrite and dolomite in the carbonate affects the pH and solution composition due to their dissolution and consequently, it could affect the interaction between crude oil and carbonate. Therefore, the mineral impurities in the carbonate should be considered in characterising the wettability alteration. This study aims to evaluate the carbonate impurities of dolomite and anhydrite on wettability alteration through coupled triple-layer surface complexation and thermodynamic equilibrium model. The zeta potential, surface complexation model, and disjoining pressure were used to assess the wettability changes in smartwater. Moreover, the calculated disjoining pressure was compared with the measured adhesion force. Finally, a sensitivity analysis was performed to evaluate the effect of crude oil surface site densities on disjoining pressure.

## 2. Model description and literature data

### 2.1 Geochemical model

To investigate the effect of carbonate impurities on wettability alteration with smartwater, the triple-layer surface complexation model built-in the geochemical code PHREEQC was used. This model could describe the electrical properties of system due to the interactions including thermodynamic reactions, dissociation of surface species and adsorption of ions. Herein, a brief description of the model is given for crude oil/brine interface and the similar model was adopted for calcite/brine interface. A detailed description of the model can be found elsewhere [9,36]. According to the previous studies [9,10,37], the carboxyl groups (–COOH) and nitrogen bases (–NH) from asphaltenes and resins are the main surface-active substances in crude oil which have a predominant effect on the electrical properties of emulsion. These two groups could determine the surface charges of emulsion

due to the dissociation and adsorption. It was assumed that both groups can affect the surface charges and thereby resulting in the formation of the triple-layer. In addition, the potential determining ions (PDIs) including magnesium and calcium ions influence the change in surface charges. The charge distribution ($\Delta z_i, i = 0,1,2$) at three layers for –NH association, –COOH dissociation, and the adsorption of magnesium, calcium, and sodium were assumed as shown in **Table 1** based on ref. [9] (**Table 2** for calcite/brine interface). The intrinsic equilibrium constants for crude oil/brine interface were calculated as follows:

$$-NH + H^+ \leftrightarrow -NH_2{}^+, \quad K_{-NH_2{}^+} = \frac{(NH_2{}^+)}{(-NH)\times a_{H^+}} \exp\left(-\frac{\Delta z_i F \varphi_i}{RT}\right) \tag{1}$$

$$-COOH \leftrightarrow -COO^- + H^+, \quad K_{-COO^-} = \frac{(-COO^-)\times a_{H^+}}{(-COOH)} \exp\left(-\frac{\Delta z_i F \varphi_i}{RT}\right) \tag{2}$$

$$-COOH + Ca^{2+} \leftrightarrow -COOCa^+ + H^+, \quad K_{-COOCa^+} = \frac{(-COOCa^+)\times a_{H^+}}{(-COOH)\times a_{Ca^{2+}}} exp\left(-\frac{\Delta z_i F \varphi_i}{RT}\right) \tag{3}$$

where $K_{-NH_2{}^+}$, $K_{-COO^-}$, and $K_{-COOCa^+}$ respect the intrinsic equilibrium constants for the protonation of nitrogen bases, the deprotonation of carboxyl groups and the adsorption of calcium respectively. Similar equations as Eq. (3) are used for magnesium and sodium adsorption as well. (–*M*) is the concentration of the surface species; $a_i$ denotes the activity of ionic species *i*; *F* is the Faraday constant equal to 96485 C·mol$^{-1}$; $\varphi_i$ is the potential of the plane-*i*; *R* is the molar gas constant equal to 8.31451 *J/(mol·K)*$^{-1}$, and *T* is the absolute temperature (*K*).

**Table 1** Charge distribution values for the dissociation and adsorption of calcium, magnesium, and sodium on crude oil

| Ions | $\Delta z_0$ | $\Delta z_1$ | $\Delta z_2$ |
|---|---|---|---|
| $OH^-$ | -1 | 0 | 0 |
| $H^+$ | 1 | 0 | 0 |
| $Ca^{2+}$ | -1 | 2 | 0 |
| $Mg^{2+}$ | -1 | 2 | 0 |

| | | | |
|---|---|---|---|
| $Na^+$ | -1 | 0 | 0 |

**Table 2** Charge distribution values for calcite/brine interface

| Ions | $\Delta z_0$ | $\Delta z_1$ | $\Delta z_2$ |
|---|---|---|---|
| $OH^-$ | -1 | 0 | 0 |
| $H^+$ | 1 | 0 | 0 |
| $Ca^{2+}$ | -1 | 2 | 0 |
| $Mg^{2+}$ | -1 | 2 | 0 |
| $Na^+$ | -1 | 0 | 0 |
| $SO_4^{2-}$ | 0 | -2 | 0 |
| $HCO_3^-$ | 0 | -1 | 0 |

The thermodynamic equilibrium between minerals and solutions were considered through "EQUILIBRIUM_PHASES" keyword in PHREEQC. The amount of minerals, the type of phase, and the specified saturation index were essential input parameters in PHREEQC. The equilibrium constant ($logK_p$) at standard condition and the standard heat of reaction ($\Delta_r H^0$) for the dissolution reactions of calcite, dolomite, and anhydrite used in the geochemical modelling were given in **Table 3** [36,38].

**Table 3** Thermodynamic properties of minerals used in the geochemical simulation

| Phase | Reactions | $logK_p$, 25°C | $\Delta_r H^0$ $(kcal/mol)$ |
|---|---|---|---|
| Calcite | $CaCO_3 \leftrightarrow {CO_3}^{2-} + Ca^{2+}$ | -8.48 | -2.970 |
| Dolomite | $CaMg(CO_3)_2 \leftrightarrow 2{CO_3}^{2-} + Ca^{2+} + Mg^{2+}$ | -17.09 | -9.436 |
| Anhydrite | $CaSO_4 \leftrightarrow {SO_4}^{2-} + Ca^{2+}$ | -4.36 | -4.037 |

## 2.2 Extended DLVO theory and disjoining pressure calculation

To further understand the interactions between crude oil and carbonate, the total disjoining pressure was used, which is comprised of van der Waals, structural and electrical forces and can be written as [11,39,40]:

$$\prod_{total}(h) = \prod_{van}(h) + \prod_{str.}(h) + \prod_{ele.}(h) \quad (8)$$

where $\prod_{total}(h)$ is the total disjoining pressure; $\prod_{van}(h)$ represents the van der Waals force; $\prod_{str.}(h)$ is the structural force, and $\prod_{ele.}(h)$ is the electrical force. The van der Waals can be calculated as follows:

$$\prod_{van}(h) = \frac{-A\,(15.96\mathrm{h}/\lambda+2)}{12\pi h^3\,(1+5.32\mathrm{h}/\lambda)^2} \quad (9)$$

where $A$ is the Hamaker constant of crude oil/brine/carbonate interface, which was assumed to be $6.6 \times 10^{-21} J$ [41]; $\lambda$ is the London wavelength, and $h$ is the separation distance of the two surfaces. The structural force is a short-range force when compared with the other two forces, which primarily acts within 1 nm [11,39]. The structural force was determined by three parameters, such as a coefficient ($A_k$), $h$, and the characteristic decay length ($h_s$), given as:

$$\prod_{str.}(h) = A_k exp(-\frac{h}{h_s}) \quad (10)$$

where the coefficient and the characteristic decay length were assumed to be $1.5 \times 10^{10} Pa$ and 0.05 nm, respectively [11,42]. The electrical force can be attractive or repulsive based on the sign of surface charge and the ionic composition in the solution. For a constant surface potential, it can be calculated as follows:

$$\Pi_{ele.}(h) = n_b k_B(\frac{2\Psi_{r1}\Psi_{r2}cosh(kh) - {\Psi_{r1}}^2 - {\Psi_{r2}}^2}{(sinh(kh))^2}) \quad (11)$$

where $n_b$ is the ion density in the bulk brine, $k_B$ is the Boltzmann constant ($1.38064 \times 10^{-23}$), $\Psi_{ri}$ is the reduced potential, and $k$ is the reciprocal Debey-Hückel double layer length. The reduced surface potential and the reciprocal of Debey-Hückel double layer length were determined by equations below:

$$\Psi_{ri} = \frac{ze\Psi_0}{k_B T} \tag{12}$$

$$k = \sqrt{\frac{2e^2 z^2 n_b}{\varepsilon_0 \varepsilon_r k_B T}} \tag{13}$$

where $z$ denotes the valence of a symmetrical electrolyte brine; $e$ is the electron change ($1.6 \times 10^{-19}$ C); $\Psi_0$ is the surface potential; $\varepsilon_0$ is the dielectric permittivity of a vacuum ($8.85 \times 10^{-12}$), and $\varepsilon_r$ represents the relative permittivity of electrolyte brine.

### 2.3 Source and application of literature experimental data

The literature data to evaluate the carbonate impurities on smartwater effect were collected from previous works [43,44] and tabulated in **Table 4**. To run the established model, key parameters including specific surface area and the surface site densities are necessary. According to the result reported by Alotaibi and Yousef [43], the oil droplets were spherical, and the mean size distribution could be obtained directly, which were used for calculating the specific surface area. However, the calcite particles were smaller with irregular shapes and their specific surface area was larger than that of oil droplets. Meanwhile, Takeya et al. (2019) proposed the logarithmic equation to estimate the site density of –COOH based on TAN at 50 ºC, and they did not provide any suggestion to estimate -NH site density [10]. In this study, the modelling was performed to fit and predict the experimental data at 22 ºC and thus, the proposed equation by Takeya et al. (2019) [10] cannot be used. Moreover, this study considered both –COOH and –NH sites in crude oil/brine/carbonate system. Therefore, for the consistency in estimating both site densities, the equations proposed by Eftekhari et al. [45] have been used to calculate the surface site densities of –COOH and –NH as follows [45]:

$$N_{S,-COOH} = \frac{0.602\times10^{6}\times TAN}{10^{3}\times a_{oil}\times MW_{KOH}} \quad (14)$$

$$N_{S,-NH} = \frac{0.602\times10^{6}\times TBN}{10^{3}\times a_{oil}\times MW_{KOH}} \quad (15)$$

where $Ns,_{-COOH}$ and $Ns,_{-NH}$ represent the carboxylic and nitrogen sites per nm$^2$ respectively; *TAN* and *TBN* are the total acid and base numbers; $a_{oil}$ is the specific surface area of the crude oil, and $MW_{KOH}$ is the molecular weight of potassium hydroxide (KOH). The natural carbonate considered in this study contained 80% calcite, 13% dolomite, 6% anhydrite and less than 1% quartz [44].

**Table 4** Brine and oil related properties and the experimental data for zeta potential and adhesion force

| Items | DI Water | Brine1 | Brine2 | Brine3 | Brine4 |
|---|---|---|---|---|---|
| pH | 7.04 | 6.32 | 6.05 | 6.27 | 6.67 |
| $Na^+$/ppm | – | – | – | 1865 | 1824 |
| $Mg^{2+}$/ppm | – | 1471 | – | – | 211 |
| $Ca^{2+}$/ppm | – | – | 2080 | – | 65 |
| $SO_4^{2+}$/ppm | – | – | – | 3896 | 429 |
| $Cl^-$ /ppm | – | 4290 | 3681 | – | 3220 |
| $HCO_3^-$ /ppm | – | – | – | – | 12 |
| TDS/ppm | 0 | 5761 | 5761 | 5761 | 5761 |
| Ionic strength/M | 0 | 0.18 | 0.16 | 0.12 | 0.12 |
| Oil droplet/μm (d) | 14.25 | 15.51 | 19.74 | 9.50 | 21.53 |
| ζ-potential/mV (oil-brine) * | -156.11 | -33.58 | -14.15 | -46.84 | -51.66 |
| ζ-potential/mV (carbonate-brine) | -27.44 | 8.92 | 12.32 | -30.15 | -10.54 |
| Adhesion force/μN (oil-brine-carbonate) | 140 | 111.4 | 110.7 | 98.9 | 103 |

*where TAN of oil is 0.19 mg/g KOH; TBN is 0.08 mg/g KOH. The zeta potential was measured at room temperature.

## 3. Results and discussion

### 3.1 Triple layer surface complexation model for crude oil/brine and carbonate/brine: Parameter optimisation and validation

In the triple layer surface complexation model, the equilibrium constants for protonation/deprotonation and ionic adsorption were determined by fitting the experimental zeta potential results with that of modelling where inner and outer capacitance of the model varies according to PDIs. From the particle size distribution of crude oil in various brines [43], the specific surface area and site densities of –COOH and –NH (eqs. (14-15)) were determined and tabulated in **Table 5**. Initially, the fitting was performed for crude oil/DI water to determine equilibrium constants ($K_{O,1}$ and $K_{O,2}$ in **Table 5**) for protonation/deprotonation. It was assumed that only water molecules were attached to inner and outer Stern layers and the calculated $C_{1,oil}$ and $C_{2,oil}$ for emulsion formed by crude oil and DI Water was 2.510 F/m$^2$. The fitting of measured zeta potential with that of predicted result is shown in **Fig. 1**, and the estimated equilibrium constants are given in **Table 5**. These values were used to estimate equilibrium constants for the adsorption of calcium, magnesium, and sodium ions ($K_{O,3}$, $K_{O,4}$, and $K_{O,5}$ in **Table 5**). For Brine1 ($MgCl_2$) and Brine2 ($CaCl_2$), the distances of the inner and outer Stern layers were respectively determined by the presence of magnesium (diameter 1.30 Å)/calcium ions (diameter 1.98 Å) and water molecules (diameter 2.75 Å), which were used to calculate inner and outer capacitance (**Table 5**). The predicted zeta potential result was fitted to measured data of each brine by only adjusting $K_{O,3}$ or $K_{O,4}$ (**Fig. 1**). To fit the zeta potential data in Brine3 ($Na_2SO_4$), the effect of sodium ion was considered because sulphate ions does not influence the potential changes at crude oil/brine interface. It was assumed that there is only water molecules in inner and outer Stern layers, and the calculated $C_{1,oil}$ and $C_{2,oil}$ were equal to 2.253 F/m$^2$ for the solution dielectric constant of 70. The estimated equilibrium constant values are tabulated in **Table 5**, which are rather smaller than those reported in literatures [9,10,37,46]. This is due to temperature difference between this study and previous studies as the equilibrium constant is a

function of temperature through Van't Hoff equation. The estimated equilibrium constants were validated in Brine4 (smartwater). The inner and outer capacitance for crude oil in smartwater is the same as the values calculated in Brine2 ($CaCl_2$) as the calcium ion is the largest one in the solution which controls the inner capacitance. The predicted zeta potential of crude oil in smartwater agreed reasonably well with the measured data (**Fig. 1**), thereby suggesting the applicability of the model and surface complexation parameters in smartwater.

**Table 5** Determined surface complexation parameters for crude oil

| Items | DI Water | Brine1 | Brine2 | Brine3 | Brine4 |
|---|---|---|---|---|---|
| ≡COOH surface site density (sites/$nm^2$) | 4.28 | 4.66 | 5.93 | 2.85 | 6.47 |
| ≡NH surface site density (sites/$nm^2$) | 1.80 | 1.96 | 2.50 | 1.20 | 2.72 |
| Specific surface area ($m^2/g$) | 0.476 | 0.437 | 0.344 | 0.714 | 0.315 |
| $C_{1,oil}$ ($F/m^2$) | 2.510 | 4.765 | 3.129 | 2.253 | 3.129 |
| $C_{2,oil}$ ($F/m^2$) | 2.510 | 2.253 | 2.253 | 2.253 | 2.253 |
| Surface reaction | $Log_{10}K$ (22 °C) | | | Value | |
| $\equiv NH + H^+ \leftrightarrow \equiv NH_2^+$ | $K_{O,1}$ | | | 2.79 | |
| $\equiv COOH \leftrightarrow \equiv COO^- + H^+$ | $K_{O,2}$ | | | -6.32 | |
| $\equiv COOH + Ca^{2+} \leftrightarrow \equiv COOCa^+ + H^+$ | $K_{O,3}$ | | | -5.42 | |
| $\equiv COOH + Mg^{2+} \leftrightarrow \equiv COOMg^+ + H^+$ | $K_{O,4}$ | | | -8.71 | |
| $\equiv COOH + Na^+ \leftrightarrow \equiv COONa + H^+$ | $K_{O,5}$ | | | -5.02 | |

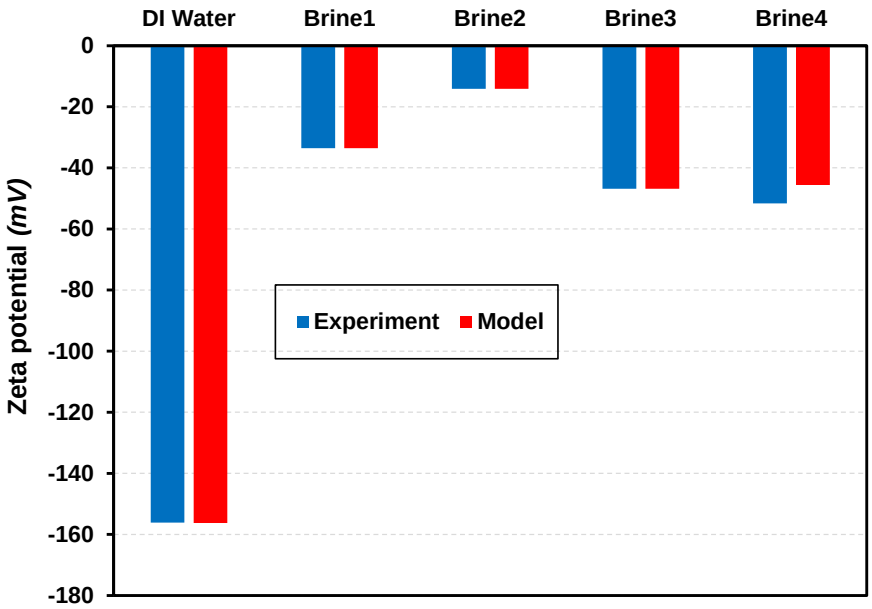


**Fig. 1.** Measured and predicted zeta potential of crude oil in DI water and brines

A similar methodology was adopted for carbonate/brine interface to optimise the equilibrium constants for surface complexation reactions. It was assumed that the surface electrical properties of carbonate/brine are governed by calcite surface. Therefore, in this study, the surface complexation modelling parameters for calcite/brine are estimated by fitting the experimental data to modelling results, where the dissolution of anhydrite and dolomite was not considered to minimise the number of fitting parameters. As reported in the previous studies [47], the calcite surface possesses >CaOH and $>CO_3H$ sites for protonation/deprotonation and adsorption of ions. The site density of both surfaces was assumed to be 4.95 sites/nm$^2$ and the specific surface area of calcite was 2.15 m$^2$/g [11]. The calcium ions from the dissolution of calcite in solution determine the inner capacitance (3.129 F/m$^2$) whereas 0.200 F/m$^2$ was assumed for outer capacitance. To predict the zeta potential of carbonate/brine, various ions have been considered and their charge distribution in the triple-layer model is given in **Table 2**. At each case, the dissolution of calcite releases calcium and carbonate ions into the solution. Therefore, the experimental data for DI Water and Brine2 ($CaCl_2$) needs to be fitted at the initial stage to determine $K_{C,1}$, $K_{C,2}$, $K_{C,3}$ and $K_{C,4}$ (**Table 6**). Afterwards, the data for Brine1 ($MgCl_2$) was fitted to estimate $K_{C,5}$, and then Brine3 ($Na_2SO_4$) was used to determine $K_{C,6}$ and $K_{C,7}$.

It should be noted that the adsorption of $HCO_3^-$ and $SO_4^{2-}$ is considered on $>CaOH_2^+$ surface [28, 47], and the appropriate charge distribution is given in **Table 2**. The optimised surface complexation modelling parameters are tabulated in **Table 6** and they are comparable to the data reported in the previous studies [11,34,39]. Finally, the modelling parameters were validated in predicting the zeta potential of smartwater and then comparing with experimental data. The fitting and prediction are shown in **Fig. 2**. As can be seen, the model was able to successfully predict the zeta potential of carbonate in smartwater.

**Table 6** Determined surface complexation parameters for carbonate core particles

| Items | | Value |
|---|---|---|
| >CaOH surface site density (sites/nm$^2$) | | 4.95 |
| $>CO_3H$ surface site density (sites/nm$^2$) | | 4.95 |
| Specific surface area (m$^2$/g) | | 2.15 |
| $C_{1,carbonate}$ (F/m$^2$) | | 3.129 |
| $C_{2,carbonate}$ (F/m$^2$) | | 0.200 |
| Surface reaction | $Log_{10}K$ (22 °C) | Value |
| $>CO_3H \leftrightarrow >CO_3^- + H^+$ | $K_{C,1}$ | -3.37 |
| $>CaOH + H^+ \leftrightarrow >CaOH_2^+$ | $K_{C,2}$ | 11.70 |
| $>CO_3H + Ca^{2+} \leftrightarrow >CO_3Ca^+ + H^+$ | $K_{C,3}$ | -1.00 |
| $>CaOH_2^+ + HCO_3^- \leftrightarrow >CaOH_3CO_3$ | $K_{C,4}$ | 5.05 |
| $>CO_3H + Mg^{2+} \leftrightarrow >CO_3Mg^+ + H^+$ | $K_{C,5}$ | 0.04 |
| $>CO_3H + Na^+ \leftrightarrow >CO_3Na + H^+$ | $K_{C,6}$ | -1.15 |
| $>CaOH_2^+ + SO_4^{2-} \leftrightarrow >CaOH_2SO_4^-$ | $K_{C,7}$ | 10.70 |

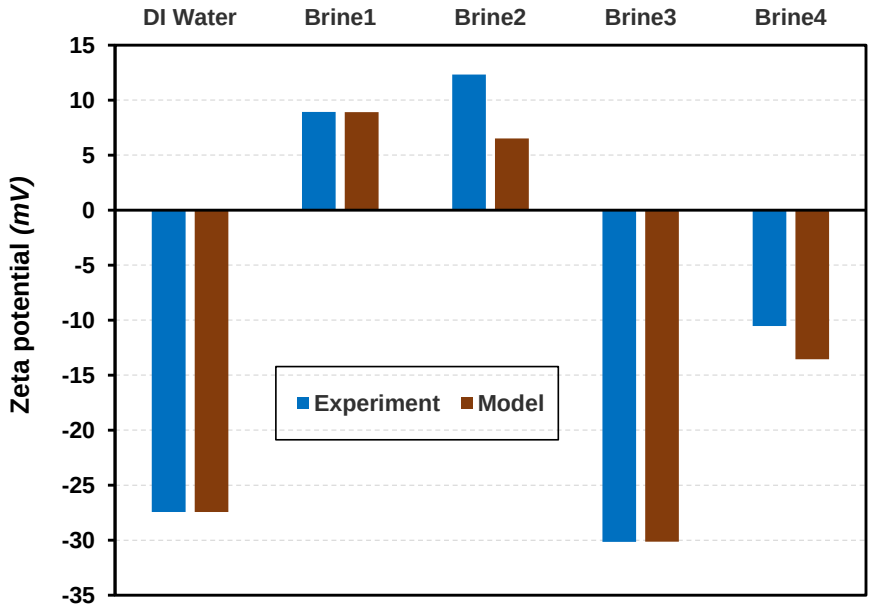


**Fig. 2.** Measured and predicted zeta potential of carbonate in DI water and brines

### 3.2 Effect of carbonate impurities on interface properties

The crushed carbonate core sample used to measure zeta potential composed of 80% calcite, 13% dolomite, 6% anhydrite, and less than 1% quartz [44]. The presence of impurities and their amount were considered in the phase-equilibrium model as given in **Table 3**. In the phase-equilibrium model, the amounts of minerals' moles were selected with respect to their composition in the carbonate for dissolution. Dolomite and anhydrite impurities dissolve into the solution and change pH and ionic composition of $Ca^{2+}$, $Mg^{2+}$, $CO_3^{2-}$ and $SO_4^{2-}$, which could influence the interface properties through the reactions given in **Table 6.** It should be noted that the surface complexation model for either dolomite or anhydrite is not considered in this study because the dissolution is more significant than surface complexation reaction for anhydrite or dolomite. **Fig. 3** shows the effect of impurities equilibrium on the calculated zeta potential of carbonate and its comparison with experimental data. The calculation was performed without considering the crude oil. The equilibrium of anhydrite releases enough sulphate ions into the solution and reverses the calculated zeta potential from positive to negative in Brine1 ($MgCl_2$) and Brine2 ($CaCl_2$) solution, which is oppositive to the measured data. It is important to note that the equilibrium of calcite or impurities of dolomite and anhydrite does not

have a significant influence on the zeta potential of carbonate in smartwater (Brine4). This is mainly due to the reason that smartwater contained enough PDIs and as a result, their compositions did not change considerably with the minerals' equilibrium.

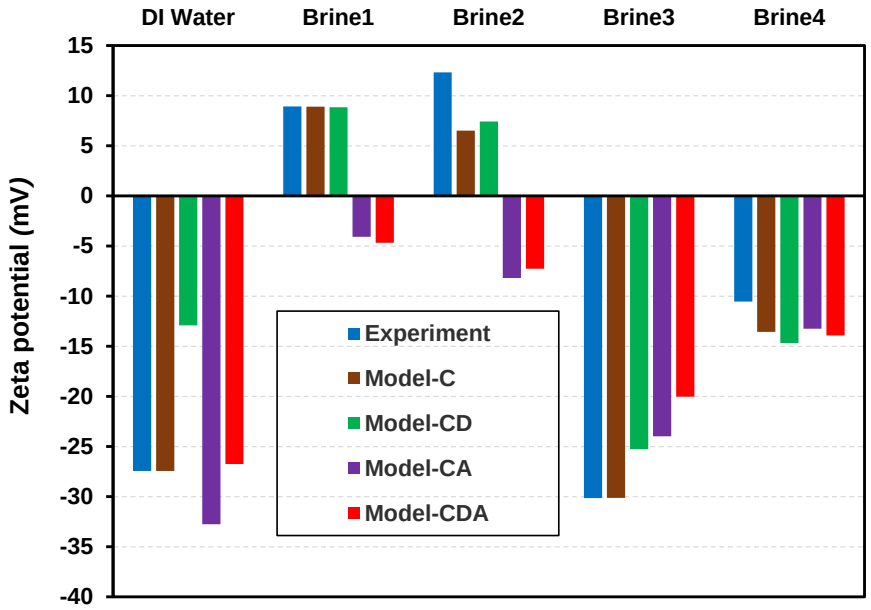


**Fig. 3.** Influence of impurities equilibrium on zeta potential of carbonate in DI water and brines. C: Equilibrium with calcite; CD: Equilibrium with calcite and dolomite; CA: Equilibrium with calcite and anhydrite; CDA: Equilibrium with calcite, dolomite, and anhydrite. [Carbonate-DI water/brines system]

A similar calculation was performed for crude oil-brine-carbonate system in the presence of crude oil. The calculated surface potential of crude oil and that of carbonate is shown in **Fig. 4**. The effect of impurities on carbonate surface potential in the presence of crude oil showed similar trend as obtained for zeta potential (**Fig. 3.**). However, the equilibrium of carbonate minerals does not remarkably affect the surface potential of crude oil, and the crude oil surface still shows negative charge. The potential variation with the equilibrium of mineral relates to pH change. For example, in Brine2 ($CaCl_2$), pH was around 9.4 when considering the equilibrium of calcite or both of calcite and dolomite, but it was reduced to 8.8 with anhydrite equilibrium. These pH variations correspond to the change of surface

potential. The distribution of surface species of crude oil and carbonate without or with the equilibrium of calcite, dolomite and anhydrite is shown in **Fig. 5.** Again, the impurities equilibrium has no effect on crude oil surface species whereas the release of sulphate ions from anhydrite equilibrium forms $>CaOH_2SO_4^-$ which controls the calcite surface. The $>CaOH_2SO_4^-$, $>CO_3Mg^+$, and $>CO_3Ca^+$ are the main surface species when the carbonate equilibrates with various solutions, where the density of $>CO_3^-$ and $>CaOH_2^+$ are negligible on calcite surface. In smartwater, the concentration of surface species is almost equal with or without impurities equilibrium, which clearly explains the independence of surface/zeta potential with impurities equilibrium for this case.

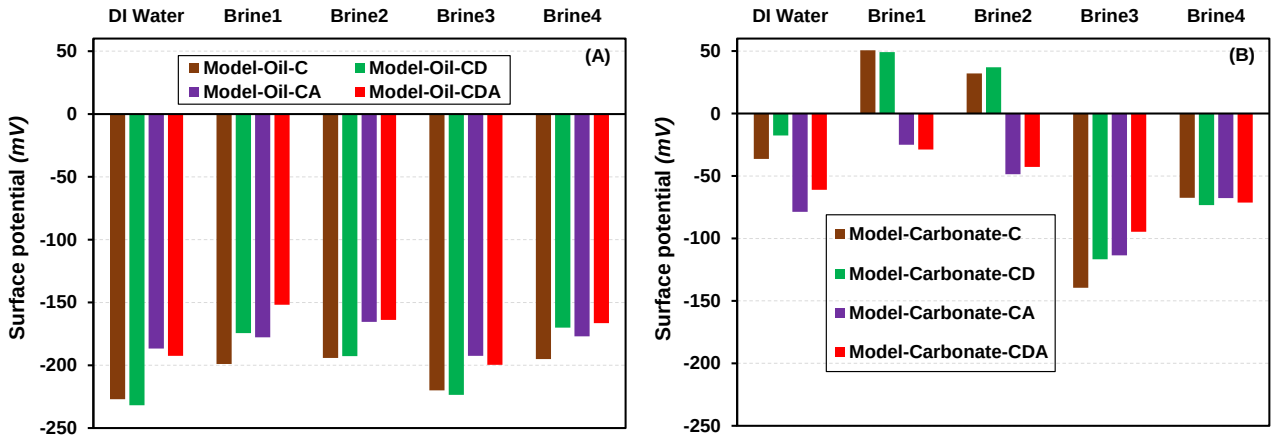


**Fig. 4.** Effect of impurities on surface potential of crude oil and carbonate in DI water and brines. (A) Surface potential of crude oil; (B) Surface potential of carbonate. C: Equilibrium with calcite; CD: Equilibrium with calcite and dolomite; CA: Equilibrium with calcite and anhydrite; CDA: Equilibrium with calcite, dolomite, and anhydrite. [Crude oil- DI water/brines- carbonate system]

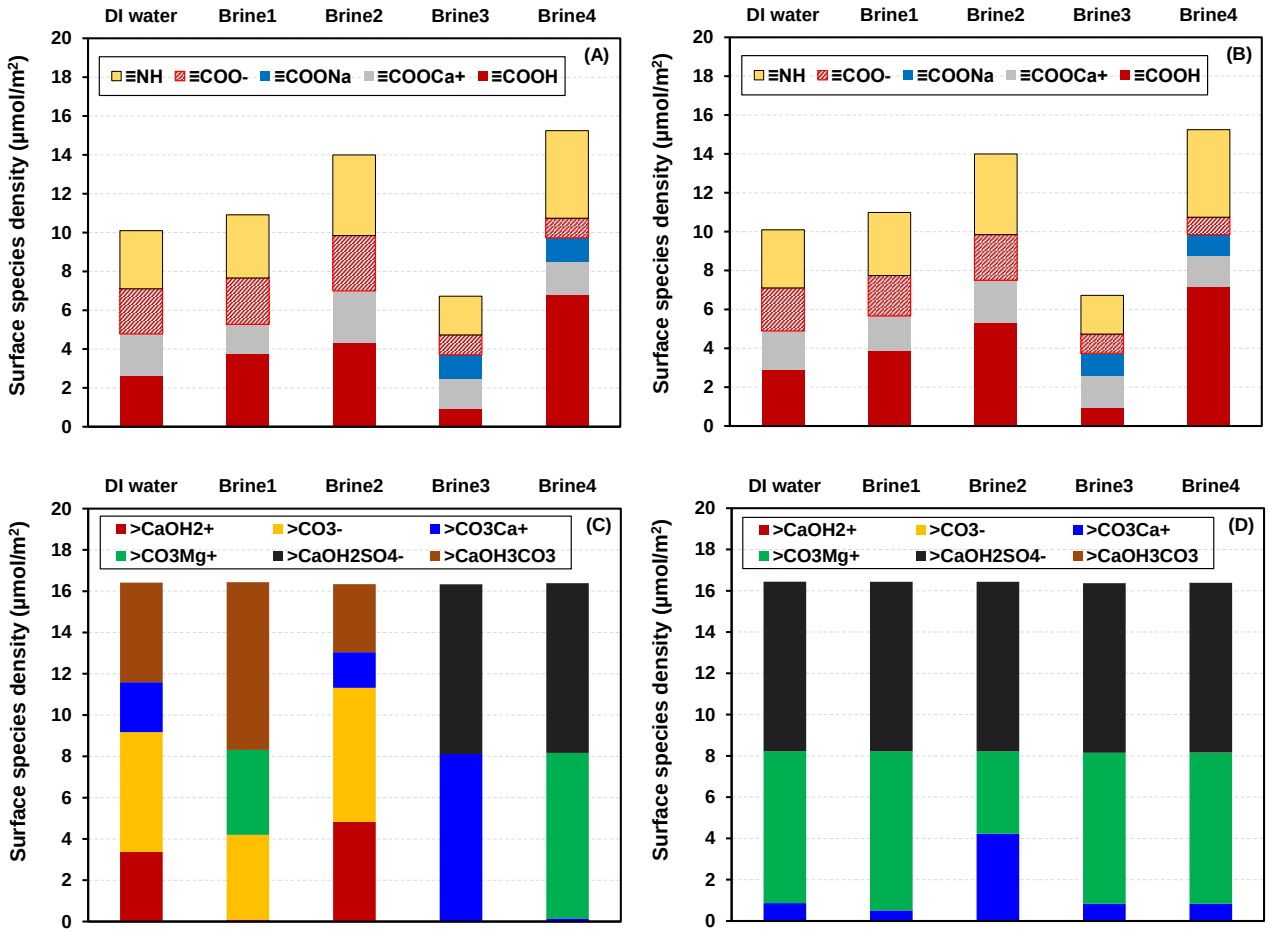


**Fig. 5** (A) Surface species density of crude oil in the system without impurities equilibrium; (B) Surface species density of crude oil in the system with the equilibrium of calcite, dolomite and anhydrite; (C) Surface species density of carbonate in the system without impurities equilibrium; (D) Surface species density of carbonate in the system with the equilibrium of calcite, dolomite and anhydrite

### 3.3 Impact of carbonate impurities and crude oil properties on disjoining pressure

The surface potentials were used to calculate total disjoining pressure which was adopted to evaluate the wettability alteration. Consistent with previous studies [11,39,41], the calculated van der Waals force was negative whereas the structural force acting at < 1nm was positive. Therefore, the electrical force controls the total disjoining pressure. The effect of impurities equilibrium on total disjoining pressure is shown in **Fig. 6**. The surface potential of crude oil was negative in DI Water/Brines (**Fig. 4**(A)). The positive surface potential of carbonate with the equilibrium of calcite or calcite and

dolomite in Brine1 and Brine2 (**Fig. 4**(B)) develops an attractive force (negative disjoining pressure) between crude oil and carbonate (**Fig. 6**(A) and (B)). However, the equilibrium of anhydrite reversed the surface potential of carbonate from positive to negative and resulted in repulsive (positive disjoining pressure) force (**Fig. 6**(C) and (D)). The calculated disjoining pressure shows repulsion between crude oil and carbonate in smartwater. Furthermore, the magnitude of disjoining pressure varied according to the surface potentials of crude oil and carbonate.

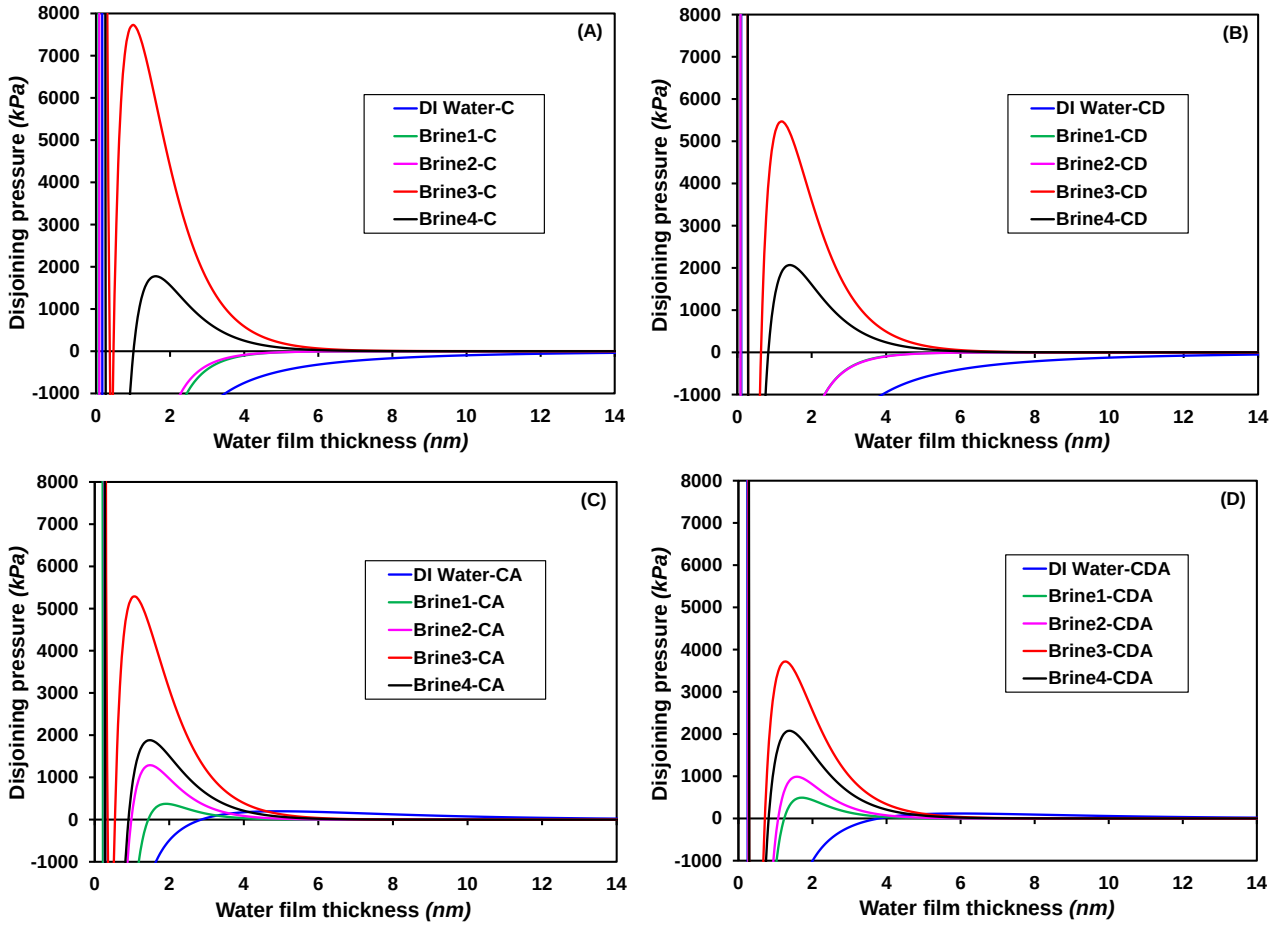


**Fig. 6** Calculated total disjoining pressure between crude oil and carbonate in DI water and brines. (A) Equilibrium with calcite; (B) Equilibrium with calcite and dolomite; (C) Equilibrium with calcite and anhydrite; (D) Equilibrium with calcite, dolomite, and anhydrite.

The positive or negative disjoining pressure was obtained due to respective repulsive or attractive forces between crude oil and carbonate in the brines (**Fig. 6.**). However, a constant positive adhesion

force was measured after the oil droplet detached from the carbonate [44]. The calculated total disjoining pressure was compared with the measured adhesion force in **Fig. 7**. As can be seen in the figure, the disjoining pressure was calculated at 1.0, 1.5 and 2.0 nm. It should be noted that the disjoining pressure was calculated considering the equilibrium of calcite, dolomite, and anhydrite. The electrical force is the main contributor to the total disjoining pressure at a separating distance higher than 1 nm. Although the measured adhesion force cannot be directly compared to the calculated disjoining pressure, the measured adhesion force shows a good relationship with the calculated disjoining pressure: high adhesion force shows low disjoining pressure or vice versa. In particular, the total disjoining pressure calculated at 1 nm exhibits a good relationship with the measured adhesion force (**Fig. 7(B)**). The disjoining pressure and adhesion force results indicate that crude oil is closely attached to carbonate in DI water. On the other hand, both the crude oil and carbonate repelled with each other in the other solutions where Brine3 ($Na_2SO_4$) shows lowest adhesion force or highest disjoining pressure. Both Brine4 (smartwater) and Brine3 ($Na_2SO_4$) have a similar ionic strength, but the higher adsorption of sulphate ions on carbonate in Brine3 ($Na_2SO_4$) shows high negative surface potential of carbonate which strongly repulses the crude oil. These results are consistent with the measured contact angle; a smaller contact angle was obtained for Brine3 ($Na_2SO_4$) [44].

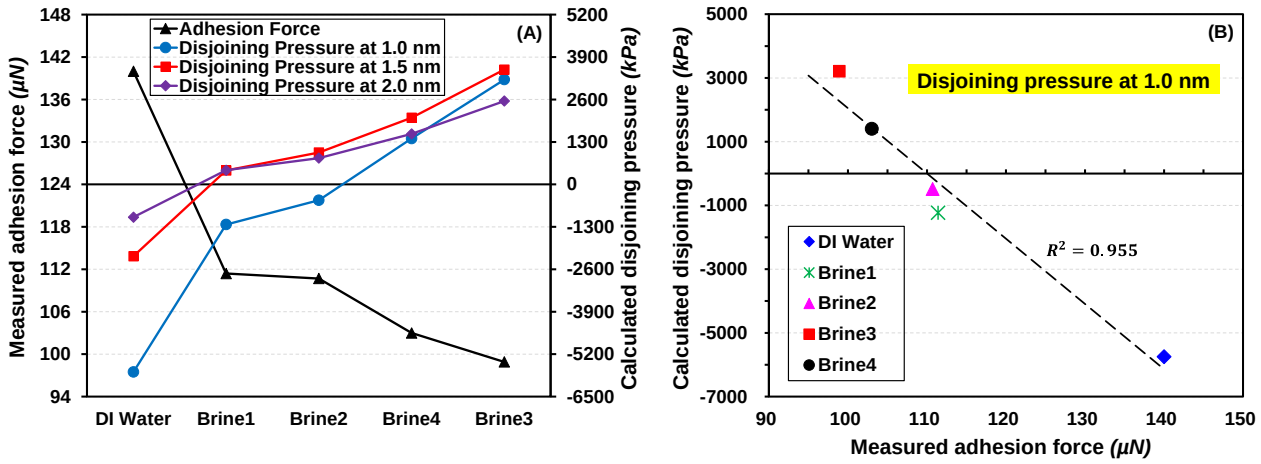


**Fig. 7** (A) Comparison of measured adhesion force with calculated disjoining pressure between crude oil and carbonate in DI water and brines; (B) The best relationship between measured adhesion force and calculated disjoining pressure at 1 nm.

The disjoining pressure is governed by electrical force or surface potential which is sensitive to the surface complexation modelling parameters given in **Table 5** and **Table 6**. Indeed, the equilibrium constant strongly influences the surface or zeta potential, which is a function of temperature and is usually derived by fitting the experimental data. In addition to equilibrium constant, the surface site density is an important factor controlling the surface electrical properties, which was determined by the structure of minerals or molecules. From the defined structure of calcite, the surface site density of calcite is constant. On the other hand, it is difficult to estimate the surface functional groups and their densities from the structure of crude oil. Eftekhari et al. [45] proposed equations (14) and (15) to estimate site densities while other researchers [10] have suggested a different method. However, the applicability of these methods to estimate surface site densities of crude oil depends on the TAN or TBN. A crude oil with TAN of 0.19 g/g KOH and TBN of 0.08 g/g KOH was used to evaluate wettability alteration using electrokinetics in this study. The effect of crude oil site densities, in other words TAN/TBN, on total disjoining pressure is shown in **Fig. 8**. The calculations were performed in smartwater with the equilibrium of impurities. The change of site densities modifies the surface potential of crude oil, and subsequently it affects the wettability alteration through the change of disjoining pressure. The calculation results indicate that higher –COOH/–NH ratio shows stronger repulsion between the crude oil and carbonate.

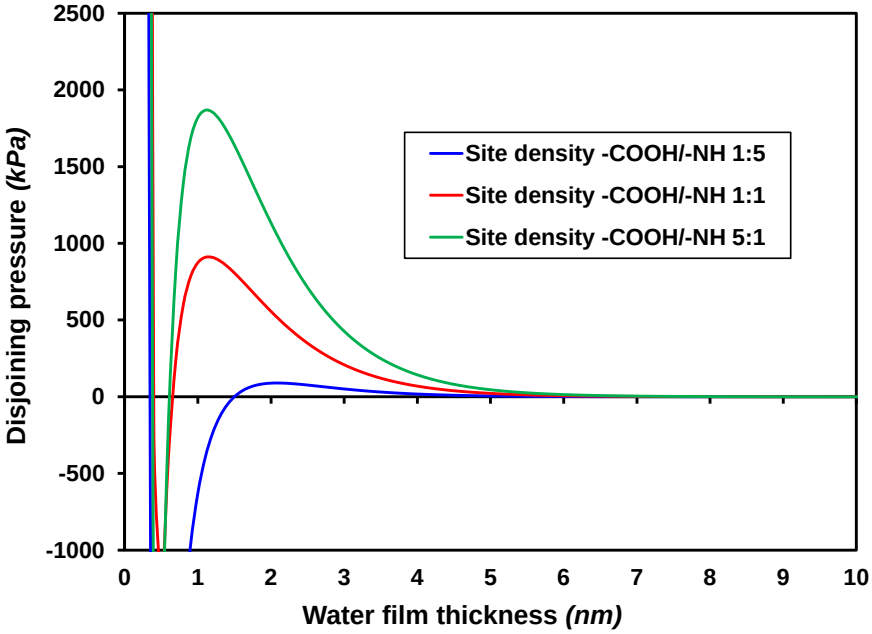


419

420 **Fig. 8.** Calculated disjoining pressure for crude oil/smartwater/carbonate system with different site
421 density ratios of –COOH and –NH.

422

423 **4. Conclusions**

424 A triple-layer surface complexation model was established and applied to predict the zeta potential
425 of crude oil and carbonate in smartwater. The model is coupled with thermodynamic equilibrium
426 reactions to analyse the carbonate impurities on wettability changes. The measured and calculated
427 zeta potentials of crude oil and carbonate in various solutions were successfully fitted to estimate the
428 equilibrium constant of reactions, and it was validated with predicting the zeta potential in smartwater.
429 The equilibrium of carbonate impurities of dolomite and anhydrite does not affect the electrokinetic
430 properties of crude oil/brine, but the equilibrium of anhydrite changes the carbonate zeta or surface
431 potential from positive to negative in $CaCl_2$ or $MgCl_2$ solution. As a result of impurities equilibrium,
432 the surface of carbonate is mainly composed of $>CaOH_2SO_4^-$ and $>CO_3Mg^+$ species, which governs
433 the potential. The impurities equilibrium has a less effect in smartwater or $Na_2SO_4$ solution that
434 contains sulphate ions. The calculated disjoining pressure is inversely correlated with measured
435 adhesion force and the highest disjoining pressure or the lowest adhesion force was obtained in
436 $Na_2SO_4$ solution. The disjoining pressure and adhesion force results show that the crude oil is closely

attached to carbonate surface in DI water, indicating oil-wet condition. This condition did not change even with the equilibrium of anhydrite. On the hand, the crude oil and carbonate have repelled with each other in $Na_2SO_4$ or smartwater, suggesting the water-wet condition. Therefore, the wettability from oil-wet to water-wet in the system was in the following order DI water > brine with $Mg^{2+}$ > brine with $Ca^{2+}$ > brine with $Ca^{2+}$, $Mg^{2+}$, and $SO_4^{2-}$ > brine with $SO_4^{2-}$. Lastly, the effect of crude oil properties on disjoining pressure was evaluated. It is found that –COOH/–NH (TAN/TBN) ratio strongly affects the disjoining pressure and wettability changes in crude oil/smartwater/carbonate system.

## CRediT authorship contribution statement

**Xingjuan Hao:** Conceptualization, Methodology, Formal analysis, Software, Writing-original Draft, Writing-review & editing. **Moataz Abu-Al-Saud:** Conceptualization, Methodology, Formal analysis, Writing-review & editing. **Subhash Ayirala:** Conceptualization, Methodology, Formal analysis, Supervision, Writing-review & editing. **Yogarajah Elakneswaran:** Conceptualization, Methodology, Formal analysis, Software, Supervision, Writing-original Draft, Writing-review & editing.

## Declaration of Competing Interest

The authors declare that they have no known competing financial interests or personal relationships that could have appeared to influence that work reported in this paper.

## Acknowledgment

We would like to express our gratitude to Ms. Mai Shimokawara from Japan Oil, Gas and Metals National Corporation (JOGMEC) for her assistance and advice on modelling.

## References


[1] H.H. Downs, P.D. Hoover, Laboratory and Field Pilot Waterflood Studies. In Oil-Field Chemistry, Enhanced Recovery and Production Simulation, ed. J. K. Borchardt and T. F. Yen, Chap. 32, 577-595. Washington, DC, USA: ACS Symposium Series Vol. 396 (1989), American Chemical Society.

[2] P.O. Roehl, P.W. Choquette, Carbonate Petroleum Reservoirs. Springer-Verlag, New York City (1985).

[3] M.H. Doranehgard, M. Siavashi, The effect of temperature dependent relative permeability on heavy oil recovery during hot water injection process using streamline-based simulation. Applied Thermal Engineering. 129 (2018) 106-116.

[4] Y. Elakneswaran, A. Ubaidah, M. Takeya, M. Shimokawara, H. Okano, Effect of electrokinetics and thermodynamic equilibrium on Low-Salinity Water Flooding for enhanced oil recovery in sandstone reservoirs. ACS Omega. 6 (5) (2021) 3727-3735.

[5] P. Raffa, A.A. Broekhuis, F. Picchioni, Polymeric surfactants for enhanced oil recovery: A review. Journal of Petroleum Science and Engineering. 145 (2016) 723-733.

[6] A. Rahimi, B. Honarvar, M. Safari, The role of salinity and aging time on carbonate reservoir in low salinity seawater and smart seawater flooding. Journal of Petroleum Science and Engineering. 187 (2020) 106739.

[7] M.M. Salehi, M.A. Safarzadeh, E. Sahraei, S.A.T. Nejad, Comparison of oil removal in surfactant alternating gas with water alternating gas, water flooding and gas flooding in secondary oil recovery process. Journal of Petroleum Science and Engineering. 120 (2014) 86-93.

[8] S.E. Siadatifar, M. Fatemi, M. Masihi, Pore scale visualization of fluid-fluid and rock-fluid interactions during low-salinity waterflooding in carbonate and sandstone representing micromodels. Journal of Petroleum Science and Engineering. 198 (2021) 108156.

[9] M. Takeya, M. Shimokawara, Y. Elakneswaran, T. Nawa, S. Takahashi, Predicting the electrokinetic properties of the crude oil/brine interface for enhanced oil recovery in low salinity waterflooding. Fuel. 235 (2019) 822-831.

[10] M. Takeya, M. Shimokawara, Y. Elakneswaran, H. Okano, T. Nawa, Effect of acid number on the electrokinetic properties of crude oil during Low-Salinity Waterflooding. Energy & Fuels. 33 (2019) 4211-4218.

[11] M. Takeya, A. Ubaidah, M. Shimokawara, H. Okano, T. Nawa, Y. Elakneswaran, Crude oil/brine/rock interface in low salinity waterflooding: Experiments, triple-layer surface complexation model, and DLVO theory. Journal of Petroleum Science and Engineering. 188 (2020) 106913.

[12] J.T. Tetteh, P.V. Brady, R.B. Ghahfarokhi, Review of Low Salinity Waterflooding in Carbonate Rock: Mechanisms, Investigation techniques, and Future Directions. Advances in Colloid and Interface Science 284 (2020) 102253.

[13] H. Guo, N. Nazari, S. Esmaeilzadeh, A.R. Kovscek, A Critical Review of the Role of Thin Liquid Films for Modified Salinity Brine Recovery Processes. Current Opinion in Colloid & Interface Science, 50 (2020) 101393.

[14] D.A. Afekare, M. Radonjic, From mineral surfaces and coreflood experiments to reservoir implementations: comprehensive review of Low-Salinity Water Flooding (LSWF). Energy & Fuels. 31 (2017) 13043-13062.

[15] V. Alvarado, G. Garcia-Olvera, P. Hoyer, T.E. Lehmann, Impact of polar components on crude oil-water interfacial film formation: A mechanisms for low-salinity waterflooding. In: Paper SPE-170807 presentation at the SPE Annual Technical Conference and Exhibition held in Amsterdam, The Netherlands, 27-29 October (2014).

[16] T. Austad, A. RezaeiDoust, T. Puntervold, Chemical Mechanism of Low Salinity Water Flooding in Sandstone Reservoirs. In: paper SPE 37236 presented at the 2010 SPE Improved Oil Recovery Symposium held in Tulsa, Oklahoma, USA, 24-28 April (2010).

[17] S.C. Ayirala, S.H. Saleh, S.M. Enezi, A.A. Yousef, Multiscale aqueous ion interactions at interfaces for enhanced understanding of controlled ionic composition Waterflooding processes in carbonates. SPE Res Eval & Eng. 23 (03) (2020) 1118-1132.

[18] Y.Q. Chen, A. Ubaidah, Y. Elakneswaran, V.J. Niasar, Q. Xie, Detecting pH and $Ca^{2+}$ increase during low salinity waterflooding in carbonate reservoirs: Implications for wettability alteration process. Journal of Molecular Liquids. 317 (2020) 114003.

[19] D.I.O. Egbe, A.J. Ghahfarokhi, M.N. Amar, O. Torsæter, Application of Low-Salinity Waterflooding in carbonate cores: A geochemical modeling study. Natural Resources Research, 30 (1) (2021) 519-542.

[20] H. Mahani, A.L. Keya, S. Berg, W.B. Bartels, R. Nasralla, W.R. Rossen, Insights into the mechanism of wettability alteration by low-salinity flooding (LSF) in carbonates. Energy & Fuels. 29 (2015) 1352-1367.

[21] E. Pouryousefy, Q. Xie, A. Saeedi, Effect of multi-component ions exchange on low salinity EOR: Coupled geochemical simulation study. Petroleum. 2 (2016) 215-224.

[22] J.J. Sheng, Critical review of low-salinity waterflooding. Journal of Petroleum Science and Engineering. 120 (2014) 216-24.

[23] M.A. Sohal, G. Thyne, E.G. Søgaard, Review of recovery mechanisms of ionically modified waterflood in carbonate reservoirs. Energy Fuels. 30 (2016) 1904-14.

[24] A.A. Yousef, S.H. Al-Saleh, A. Al-Kaabi, M. Al-Jawfi, Laboratory investigation of the impact of injection-water salinity and ionic content on oil recovery from carbonate reservoirs. SPE Res Eval & Eng. 14 (05) (2011) 578-593.

[25] M. Karimi, R.S. Al-Maamari, S. Ayatollahi, N. Mehranbod, Wettability alteration and oil recovery by spontaneous imbibition of low salinity brine into carbonates: Impact of $Mg^{2+}$, $SO_4^{2+}$ and cationic surfactant. Journal of Petroleum Science and Engineering. 147 (2016) 560-569.

[26] P. Purswani, Z.T. Karpyn, Laboratory investigation of chemical mechanisms driving oil recovery from oil-wet carbonate rocks. Fuel. 235 (2019) 406-415.

[27] J.A.D. Dickson, Carbonate mineralogy and chemistry. In Carbonate Sedimentology (eds. Tucker, M. E. & Wright, V. P.). 284-313 (Blackwell Science, 1990).

[28] J. Song, Q. Wang, I. Shaik, M. Puerto, P. Bikkina, C. Aichele, S.L. Biswal, G.J. Hirasaki, Effect of salinity, $Mg^{2+}$ and $SO_4^{2-}$ on "smart water"-induced carbonate wettability alteration in a model oil system. Journal of Colloid and Interface Science. 563 (2020) 145-155.

[29] A. Alroudhan, J. Vinogradov, M.D. Jackson, Zeta potential of intact natural limestone: Impact of potential-determined ions Ca, Mg and SO4. Colloids and Surfaces A: Physicochemical and Engineering Aspects. 493 (2016) 83-98.

[30] J.T. Tetteh, S. Alimoradi, P.V. Brady, R.B. Ghahfarokhi, Electrokinetics at Calcite-rich Limestone Surface: Understanding the Role of Ions in Modified Salinity Waterflooding. Journal of Molecular Liquids, 297 (2020) 111868.

[31] J.T. Tetteh, M. Veisi, P.V. Brady, R.B. Ghahfarokhi, Surface Reactivity Analysis of the Crude Oil-Brine-Limestone Interface for a Comprehensive Understanding of the Low-Salinity Waterflooding Mechanism. Energy Fuels, 34 (3) (2020) 2739-2756.

[32] H. Mahani, L.K. Arsene, B. Steffen, N. Ramez, Electrokinetics of Carbonate/Brine Interface in Low-Salinity Waterflooding: Effect of Brine Salinity,Composition, Rock Type, and pH on ζ-Potential and a Surface-Complexation Model. SPE Journal, 22 (01) (2016) 53-68.

[33] P.V. Brady, G. Thyne, Functional Wettability in Carbonate Reservoirs. Energy Fuels, 30 (11) (2016) 9217-9225.

[34] Y.Q. Chen, Q. Xie, A. Sari, P.V. Brady, A. Saeedi, Oil/Water/Rock Wettability: Influencing Factors and Implications for Low Salinity Water Flooding in Carbonate Reservoirs. Fuel, 215 (2018) 171-177.

[35] J. Song, S. Rezaee, L.L. Zhang, Z.Q. Zhang, M. Puerto, O.B. Wani, F. Vargas, S. Alhassan, S.L. Biswal, G.J. Hirasaki, Characterizing the influence of organic carboxylic acids and inorganic silica impurities on the surface charge of natural carbonates using an extended surface complexation model. Energy & Fuels. 33 (2019) 957-967.

565 [36] D.L. Parkhust, C.A.J. Appelo, A computer program for speciation, batch-reaction, one-
566 dimensional transport and inverse geochemical calculations, USGS Report (1999).
567 [37] M. Bonto, A.A. Eftekhari, H.M. Nick, An overview of the oil-brine interfacial behavior and a
568 new surface complexation model. Scientific Report. 9 (2019) 6072.
569 [38] M. Shimokawara, Y. Elakneswaran, T. Nawa, S., Takahashi, Influence of carbonated water-rock
570 interactions on enhanced oil recovery in carbonate reservoirs: experimental investigation and
571 geochemical modelling. Journal of the Japan Petroleum Institute. 62 (1) (2019) 19-27.
572 [39] A. Sanaei, A. Tavassoli, K. Sepehrnoori, Investigation of modified Water chemistry for
573 improved oil recovery: application of DLVO theory and surface complexation model. Colloids
574 Surface. 574 (2019) 131-145.
575 [40] Q. Xie, Y.Q. Chen, L.J. You, M.M. Hossain, A. Saeedi, Drivers of wettability alteration for
576 oil/brine/kaolinite system: Implications for hydraulic fracturing fluids uptake in Shale Rocks.
577 Energies. 11 (7) (2018) 1666.
578 [41] A.N. Awolayo, H.K. Sarma, L.X. Nghiem, Modeling the characteristic thermodynamic interplay
579 between potential determining ions during brine-dependent recovery process in carbonate rocks.
580 Fuel. 224 (2018) 701-717.
581 [42] G.J. Hirasaki, Wettability: Fundamentals and Surface Forces. SPE Formation Evaluation. 6 (02)
582 (1991) 217-226.
583 [43] M.B. Alotaibi, A.A. Yousef, The role of individual and combined ions in waterflooding
584 carbonate reservoirs: Electrokinetic study. SPE Reservoir Evaluation & Engineering. 20 (01)
585 (2017) 077-086.
586 [44] Z.L. Li, Z.H. Xu, S. Ayirala, A. Yousef, Smartwater effects on wettability, adhesion, and oil
587 liberation in carbonates. SPE Journal. 25 (04) (2020) 1771-1783.
588 [45] A.A. Eftekhari, K. Tomsen, E.H. Stenby, H.M. Nick, Termodynamic analysis of chalk-brine-oil
589 interactions. Energy and Fuels. 31 (2017) 11773-11782.

590 [46] A.O. Alghamdi, M.O. Abu-Al-Saud, M.B. Al-Otaibi, S.C. Ayirala, A. Alyousef, Electro-kinetic
591 induced wettability alteration in carbonate: Tailored water chemistry and alkali effects. Colloids
592 and Surfaces A: Physicochemical and Engineering Aspects, 583 (2019) p.123887.
593 [47] F. Heberling, D. Bosbach, J. Eckhardt, U. Fischer, J. Glowacky, M. Haist, U. Kramar, S. Loos,
594 Reactivity of the calcite-water-interface, from molecular scale processes to geochemical
595 engineering. Appl. Geochem. 45 (2014) 158-190.